THE ASTROPHYSICAL JOURNAL, 458:L00-L00, 1996

HUBBLE SPACE TELESCOPE SPECTROSCOPIC EVIDENCE FOR A 2×10^9-M$_\odot$ BLACK HOLE IN NGC 3115[1]

JOHN KORMENDY,[2, 3] RALF BENDER,[4] DOUGLAS RICHSTONE,[5] E. A. AJHAR,[6] ALAN DRESSLER,[7]
S. M. FABER,[8] KARL GEBHARDT,[5] CARL GRILLMAIR,[8] TOD R. LAUER,[6] AND SCOTT TREMAINE[9]
Received 1995, October 31; accepted 1995, December 8

ABSTRACT

The discovery by Kormendy and Richstone of a $M_\bullet \simeq 10^9$ M$_\odot$ massive dark object (MDO) in NGC 3115 is confirmed with higher-resolution spectroscopy from the Canada-France-Hawaii Telescope (CFHT) and the *Hubble Space Telescope* (*HST*). Measurements with the CFHT and Subarcsecond Imaging Spectrograph improve the resolution from $\sigma_* = 0''.44$ to $0''.244$ (σ_* = Gaussian dispersion radius of the point-spread function [PSF]). The apparent central velocity dispersion rises from $\sigma = 295 \pm 9$ km s^{-1} to 343 ± 19 km s^{-1}. The Faint Object Spectrograph (FOS) and COSTAR-corrected *HST* provide a further improvement in resolution using a $0''.21$ aperture. Then the measured $\sigma = 443 \pm 18$ km s^{-1} is remarkably high, and the wings of the velocity profiles extend beyond 1200 km s^{-1} from the line centers. Similarly, the apparent rotation curve rises much more rapidly than from the ground. Published dynamical models fit the new observations reasonably well when "observed" at the improved spatial resolution; V and σ are at the high end of the predicted range near the center. Therefore $M_\bullet > 10^9$ M$_\odot$. The spatial resolution has now improved by a factor of ~ 5 since the discovery observations, and the case for a central MDO has strengthened correspondingly. With *HST* and the Second Wide Field and Planetary Camera (WFPC2), NGC 3115 also shows a bright nucleus. This is very prominent and distinct from the bulge when the superposed nuclear disk is subtracted. After bulge subtraction, the nucleus has $\sigma = 600 \pm 37$ km s^{-1}, the largest central dispersion seen in any galaxy. If the nucleus contained only old stars and not an MDO, its escape velocity would be ~ 352 km s^{-1}, much smaller than the observed velocities of the stars. This is independent proof that an MDO is present. The new observations put more stringent constraints on the radius inside which the dark mass lies and strengthen the case that it is a 2×10^9-M$_\odot$ black hole (BH).

Subject headings: black hole physics – galaxies: individual (NGC 3115) – galaxies: kinematics and dynamics – galaxies: nuclei

1. INTRODUCTION

Eight galaxies are now known to show stellar- or gas-dynamical evidence for central dark objects, probably BHs such as those postulated as engines for nuclear activity (see Kormendy & Richstone 1995 for a review). After M 31 (Dressler & Richstone 1988; Kormendy 1988), the edge-on S0 galaxy NGC 3115 is the best stellar-dynamical candidate (Kormendy & Richstone 1992, hereafter KR92). What this subject needs next is a large improvement in spatial resolution to see whether the BH case gets stronger or weaker. This is a prime mission of *HST*.

This paper reports *HST* FOS spectroscopy of NGC 3115 at four radii $|r| \leq 0''.30$. Also, improved CFHT spectroscopy allows us to tie these results securely to ground-based measurements. A later paper will present new dynamical models of these data and of *HST* WFPC2 images (Kormendy *et al.* 1996). Here we compare our new results with the observations and dynamical models presented in KR92. This already shows that the new spectroscopy confirms the BH detection in NGC 3115.

2. CFHT SIS SPECTROSCOPY

The Subarcsecond Imaging Spectrograph (SIS) removes the biggest limitation on Kormendy's (1988; KR92) BH spectroscopy: Herzberg Spectrograph resolution was limited by the camera optics to FWHM $\geq 0''.7$. SIS optics are better than the seeing. The scale is $0''.0864$ pixel^{-1}; a slit width of $0''.26$ was used. Tip-tilt guiding is incorporated; by offsetting the guide probe, we can center the object on the slit to one-pixel accuracy. As a result, the resolution is limited only by seeing and telescope aberrations. For NGC 3115, a lucky coincidence let us measure the PSF simultaneously with the object spectrum; normally this is not possible. A bright star near the major axis is close enough to the center so we could cut a slit that has a $4''$ square hole centered on the star. The observed width of the star spectrum then gives σ_* in the direction along the slit, and the width of the star's spectral lines (which should correspond to $\sigma = 0$ km s^{-1} except for the PSF and guiding errors) gives σ_* perpendicular to the slit. The values are $\sigma_* = 0''.244 \pm 0''.006$ and $0''.243 \pm 0''.023$. We adopt $\sigma_* = 0''.244 \pm 0''.015$ or FWHM $= 0''.57 \pm 0''.03$. This is a 45 % improvement over $\sigma_* = 0''.44$ in KR92.

The spectra were taken near the Ca II infrared triplet, at 7975 – 8975 Å. The reciprocal dispersion was 0.98 Å pixel^{-1} = 34.6 km s^{-1} pixel^{-1}. The slit length was $2'.5$, long enough to allow sky-subtraction. The results in § 4 are based on two integrations totalling 1 hr. The resolution quoted above was measured on the summed spectrum, so it includes any errors in registering the spectra.

[1] Based on observations with the NASA/ESA *Hubble Space Telescope*, obtained at the Space Telescope Science Institute, which is operated by AURA, Inc., under NASA contract NAS 5-26555.

[2] Visiting Astronomer, Canada–France–Hawaii Telescope, operated by the National Research Council of Canada, the Centre National de la Recherche Scientifique of France, and the University of Hawaii.

[3] Institute for Astronomy, University of Hawaii, 2680 Woodlawn Dr., Honolulu, HI 96822.

[4] Universitäts-Sternwarte, Scheinerstraße 1, München 81679, Germany.

[5] Dept. of Astronomy, University of Michigan, Ann Arbor, MI 48109.

[6] Kitt Peak National Observatory, National Optical Astronomy Observatories, P. O. Box 26732, Tucson, AZ 85726.

[7] Carnegie Observatories, 813 Santa Barbara St., Pasadena, CA 91101.

[8] UCO/Lick Observatory, Univ. of California, Santa Cruz, CA 95064.

[9] Canadian Institute for Theoretical Astrophysics, University of Toronto, 60 St. George St., Toronto M5S 1A7, Canada.

3. *HST* FOS SPECTROSCOPY

NGC 3115 was observed between 1994, December 27 and December 31 at four positions along the disk major axis with the $0\farcs21$ square aperture ("`0.25-PAIR`") and FOS: radii $r = 0\farcs01$, $0\farcs20$ on the SW side, and $0\farcs12$ and $0\farcs29$ on the NE side. The integration times were 129, 247, 210, and 145 min, respectively. With the red digicon and grating G570H, these exposures were designed to provide signal-to-noise ratios of ~ 50 Å^{-1}. This is sufficient to let us measure line-of-sight velocity distributions (LOSVDs).

The wavelength range, 4566 – 6815 Å, includes the Mg I *b* lines at $\lambda \simeq 5175$ Å and the Na I D lines at $\lambda \simeq 5892$ Å. The spectrum was electronically quarter-stepped, giving 2064, 1/4-diode pixels. The reciprocal dispersion was 1.09 Å pixel^{-1}. The instrumental velocity dispersion was measured using the comparison spectrum for the $r = 0\farcs0$ exposure: FWHM/2.35 $= \sigma_{\rm instr} = 1.76 \pm 0.03$ pixels $= 101 \pm 2$ km s^{-1} (internal error). This line width is intrinsic to the instrument; it is not strongly affected by the aperture illumination (Keyes *et al.* 1995, Table 1-5). Aperture illumination corrections to σ were calculated using our WFPC2 image of NGC 3115; they are $\lesssim 3$ km s^{-1}. Aperture corrections to the velocities are discussed below.

The trickiest steps in the reduction are flat-fielding and correction for geomagnetically induced motions (GIM). A flat-field image was kindly provided by C. Keyes based on a star measured with the lower `0.25-PAIR` aperture. Flat-fielding is critical because the diode response features look like narrow absorption lines (Keyes *et al.* 1995, Fig. G4). The exposure at each aperture position was divided into 4 – 8 subintegrations (orbits). The GIM shifts between different subintegrations in a series are small, but the shift between each series and the flat-field exposure is large. Therefore, we first averaged the exposures in each series and used cross-correlation to determine the shift between this average and the flat-field image. Measured shifts were 2.73 to 3.40 pixels and are accurate to $\lesssim 0.1$ pixel. Each subintegration was multiplied by the flat-field frame shifted by the above amount. Then GIM-induced shifts between subintegrations were determined; most shifts were a few tenths of a pixel; the largest was 1.25 pixels. Each subintegration was shifted to agree with the first in the series, i. e., the one closest in time to the comparison spectrum exposure. Then the spectra were added, weighted by exposure time. No problems with noisy or dead diodes required correction.

The spectra were then resampled on a $\log \lambda$ scale so that 4567 – 6800 Å cover 2048 pixels. The reciprocal dispersion is 1.0837 Å pixel^{-1} = 58.3 km s^{-1} pixel^{-1}.

Measured velocities depend on aperture illumination: if a star in the aperture is moved in the dispersion direction, V varies with position by 757 km s^{-1} arcsec^{-1}. This is predicted from the diode size ($0\farcs0770$) and was verified by measuring velocity differences for a series of spectra of a star offset by $-1\farcs46$ to $+1\farcs31$ in the $3\farcs66 \times 3\farcs71$ aperture. For our spectra, the corrections for asymmetrical aperture illumination are small: NGC 3115 was, to within $3\fdg2$, moved perpendicular to the dispersion direction. We corrected for miscentering of the galaxy in the aperture using the final peakup intensity array; corrections to V are ≤ 8 km s^{-1}, and corrections to r are $\leq 0\farcs032$.

Velocities and velocity dispersions were calculated with the same Fourier quotient program that was used in KR92. We also calculated V, σ, the higher-order Gauss-Hermite coefficients h_3 and h_4, and nonparametric LOSVDs using Bender's (1990) Fourier correlation quotient program. The two programs agree well. Velocities and dispersions are illustrated in Fig. 1 and 2; LOSVDs are shown in Fig. 3.

4. RESULTS: COMPARISON WITH KR92 MODELS

Figures 1 and 2 show that, as resolution improves, the apparent rotation curve rises more steeply to its asymptotic value $V \simeq 180$ km s^{-1}. The dispersion profile changes little at $r > 0\farcs5$, but near the center, σ increases rapidly as σ_* decreases. For example, the apparent central dispersion rises from 295 ± 9 km s^{-1} at $\sigma_* = 0\farcs44$ to 343 ± 19 km s^{-1} at $\sigma_* = 0\farcs244$. NGC 3115 contains a prominent nucleus (Fig. 4, below); there are clear signs in the SIS data that the nucleus is very hot.

FOS dramatically confirms this. The spectra at $r = 0\farcs20$ and $0\farcs30$ do not include the nucleus; they give $\sigma = 345 \pm 14$ and 318 ± 14 km s^{-1}. This is just slightly larger than the values given by SIS, a reassuring demonstration that there are no large systematic errors between the HST and ground-based results. But the two spectra that include the nucleus give *much* higher dispersions, $\sigma = 406 \pm 16$ and 443 ± 18 km s^{-1}. The nucleus is *much* hotter than its surroundings. Also, the HST spectra show a very steep central rise in the rotation curve. We now know that NGC 3115 contains an edge-on nuclear disk (Lauer *et al.* 1995; Fig. 4, below); evidently this disk rotates rapidly.

How do these observations affect the BH case? New dynamical models will be published together with all of the data in Kormendy *et al.* (1996). But the essential results already emerge from a comparison of the new data with the models presented in KR92.

KR92 computed models of NGC 3115 that bracket the observations after projection and seeing convolution. Each model consists of an unprojected rotation curve, a velocity dispersion profile, and a volume brightness profile. Some models include velocity anisotropy. We begin with isotropic models D1 – D5. They have decreasing maximum V and σ values; D3 fitted the KR92 data well; D1 and D2 had too much rotation and velocity dispersion near the center, and D4 and D5 had too little [KR92, Fig. 14; cf. Fig. 1 (*left*) here]. That is, D1+2 and D4+5 provide high- and low-$M_\bullet$ error bars, respectively. All five models imply that mass-to-light ratios rise inside $r \simeq 2''$ to values $M/L_V > 50$ that are much larger than those of old stellar populations. If the M/L_V gradient is due to a massive dark object (MDO) added to stars with constant $M/L_V(r)$, then models D1 – D5 imply $M_\bullet \simeq (3.5, 3.4, 3.0, 2.8, 2.6) \times 10^9$ M$_\odot$, respectively. These values are slightly too large, because they do not include flattening corrections. The case for an MDO was strong even at resolution $\sigma_* = 0\farcs44$: M/L_V has already risen by a factor of 5 at $r = 1''$ (see Fig. 15 in KR92). Figure 1 (*left*) compares the SIS observations with models D1 – D5 "reobserved" at the present resolution. At $r > 0\farcs2$, they bracket the new observations as they did those in KR92. But the central dispersion is higher than predicted (the reason is that the models do not contain a nucleus). So a 45% improvement in spatial resolution has increased the robustness of the MDO case.

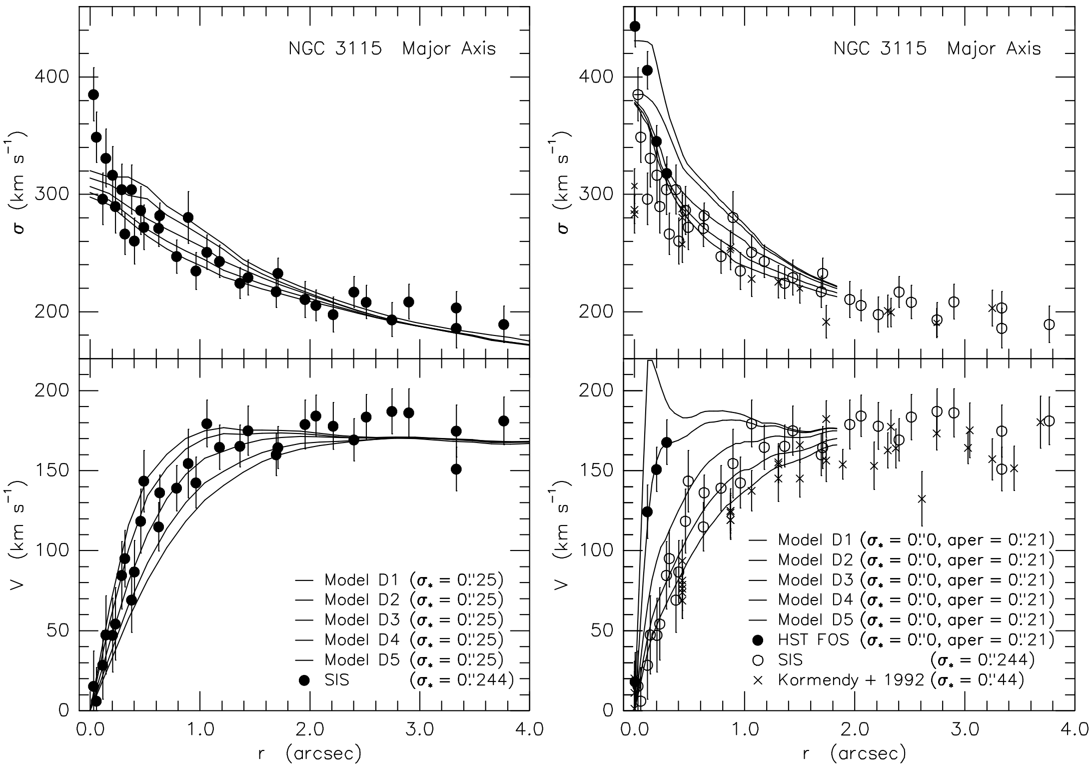

FIG. 1.—Kinematics of NGC 3115 compared with isotropic models D1 – D5 from KR92. (*left*) CFHT data plus the models as recomputed at SIS resolution. (*right*) *HST* measurements compared with the same models observed at FOS resolution. Also, crosses show the BH discovery measurements at $\sigma_* = 0\farcs44$. This figure illustrates (i) how much the apparent velocities and dispersions grow near the center as resolution improves, and (ii) how much more strongly we discriminate between models at *HST* resolution.

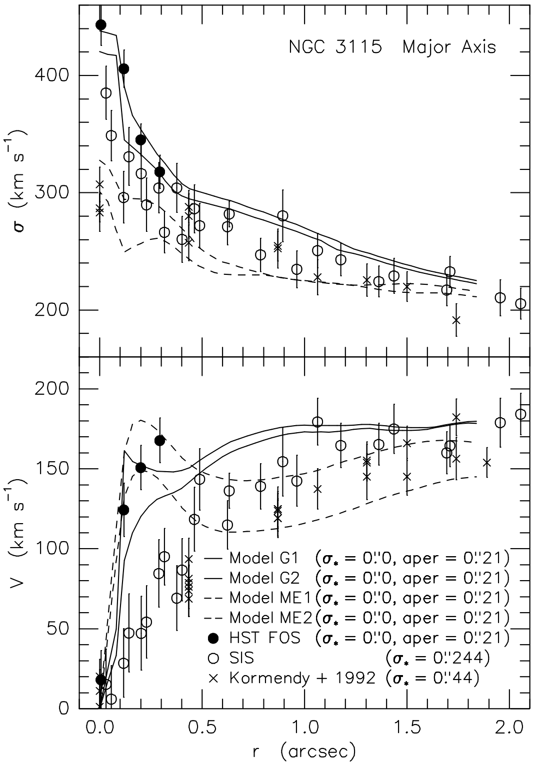

FIG. 2.—Kinematics of NGC 3115 compared with two isotropic models with point nuclei (G1 and G2) and with two anisotropic maximum entropy models from KR92.

HST improves the resolution by a further factor of 2.5. Figure 1 (*right*) shows models D1 – D5 at FOS resolution. The observed velocities are higher than the formerly best model predicts: D3 fits the dispersion profile at $0\farcs2 - 0\farcs3$, but it has too little rotation. On the other hand, V has only one component, while σ has three. So the total kinetic energy is not badly fit. The best fit to $V(r)$ is D2; the best overall fit would be intermediate between D2 and D3. All of these models imply an MDO. But their light distribution does not contain a nucleus. Not surprisingly, such models cannot reproduce the jump in σ near the center.

KR92 derived two sets of isotropic models with nuclei. We have recomputed both as observed at FOS resolution. Models J1 – J5, with a nucleus of magnitude $V = 15.94$, are excluded. The best-fitting models of the G series are shown in Fig. 2. Remarkably, model G1 is a reasonable fit to both $V(r)$ and $\sigma(r)$. In particular, it reproduces the jump in σ near the center. Its nucleus has $V = 16.53$ and $\sigma = 460$ km s^{-1}. Models G1 and G2 imply $M_\bullet = (3.5, 3.4) \times 10^9$ M$_\odot$ before flattening corrections. The reasonable agreement of the high-$M_\bullet$ isotropic models with data taken at resolution 5 times better than the σ_* for which they were derived confirms that the modeling techniques used in past BH papers are reliable.

KR92 also made anisotropic maximum entropy models (Richstone & Tremaine 1988) to see whether the need for an MDO could be removed by allowing the radial velocity dispersion to be larger than the azimuthal components. Models ME1 and ME2 reobserved at FOS resolution are shown by the dashed lines in Fig. 2. ME1 was the best attempt to fit the KR92 data without a BH. It failed by a modest amount to have enough rotation at $r \simeq 1\farcs5$. It is strongly excluded now. ME2 is the maximally anisotropic, smallest-$M_\bullet$ model that fit the KR92 data. It has $M_\bullet = 1 \times 10^8$ M$_\odot$. It, too, is excluded. Model ME3 (not shown) is similarly excluded. It has $M_\bullet = 1.4 \times 10^9$ M$_\odot$ (corrected for flattening). We conclude (i) that the BH case is much stronger at SIS and FOS resolution, and (ii) that the low-$M_\bullet$ end of the mass range allowed in KR92 is now excluded. In particular, the failure of model ME3 implies that $M_\bullet \simeq 2 \times 10^9$ M$_\odot$. Fig. 1 and 2 demonstrate how much better we can discriminate between dynamical models at FOS resolution than we could from the ground.

5. LINE-OF-SIGHT VELOCITY DISTRIBUTIONS

Further proof of the MDO is provided by the LOSVDs. The Fourier correlation quotient program provides a nonparametric measure of the LOSVDs. Figure 3 shows the result at $r = 0\farcs0$, together with the spectrum fitted by the standard star spectrum broadened by the LOSVD.

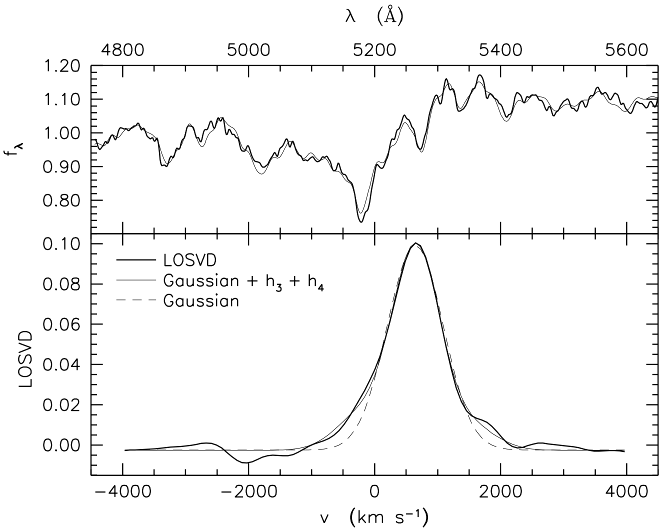

FIG. 3.—(*bottom*) Line-of-sight velocity distribution for the central FOS spectrum of NGC 3115. The curves are the Gaussian fit given by the Fourier quotient program and one that includes h_3 and h_4. Note that the Fourier quotient program is blind to the LOSVD wings. (*top*) Blue part of the spectrum and the fit of the broadened, redshifted star spectrum.

The important result is this: the line profiles have very broad wings. We derive $h_4 = 0.10 \pm 0.03$, so the LOSVD is more triangular than Gaussian. In fact, h_4 is larger than values normally seen in elliptical galaxies (Bender, Saglia, & Gerhard 1994). At ground-based resolution, not even the well-known BH candidates have such large h_4 values (van der Marel *et al.* 1994). So the nucleus contains stars whose velocities are at least 1200 km s^{-1} from the mean.

The wings of the central LOSVD provide an independent argument for an MDO. Without an MDO, the wings must arise from stars in a dense central subcluster with 10 – 20 % of the luminosity of the nucleus and a velocity dispersion of $\sim$ 1000 km s^{-1}. The nucleus has $V = 16.9$ (§ 6); at a distance of 8.4 Mpc (Kormendy & Richstone 1995), this corresponds to a luminosity of $L_V \simeq 1.2 \times 10^7$ L$_\odot$. If the nucleus consisted only of stars like those in the bulge, then $M/L_V \simeq 3.1$ (KR92), so the subcluster would have mass $\simeq 5 \times 10^6$ M$_\odot$. The dispersion and mass of the subcluster imply through the virial theorem that its median radius is $\simeq$ 0.003 pc; its relaxation time is $\sim 5 \times 10^4$ yr and the collision time between its main-sequence stars is even shorter. The subcluster could not survive. So most stars in the nucleus live near its half-light radius, $r_h \simeq 2$ pc (§ 6).

The nucleus is sharply bounded at $r_n = 0\farcs12$. Its outer volume density is at least as steep as r^{-3}, so its stars do not visit $r \gg r_n$. Without an MDO, the escape velocity at r_h would be 352 ± 27 km s^{-1}. Thus (1) fewer than half of the nuclear stars can have speeds > 352 km s^{-1}. Not including wings, the bulge-subtracted LOSVD is well fitted by a Gaussian with a remarkable dispersion of 600 ± 37 km s^{-1}. If the nucleus is spherical, then (2) 96 % of the stars have speeds > 352 km s^{-1}. (3) Even line-of-sight speeds are > 352 km s^{-1} for 56 % of the stars, plus most of those in the LOSVD wings. Both (2) and (3) contradict (1). Therefore, independent of velocity anisotropy, stars are moving too quickly to be in dynamical equilibrium by themselves. At 600 km s^{-1}, the nuclear crossing time is 15,800 y. Without an MDO, the nucleus would explode.

6. PROPERTIES OF THE NUCLEUS: IS THE MDO A BH?

Fig. 4 shows a photometric decomposition of NGC 3115 into bulge and nuclear disk. Projected at inclination 81$\fdg$0 on the center, the disk hides the nucleus. The middle image and the residual brightness profiles show that the nucleus stands out dramatically above the bulge (cf. M 31, Lauer *et al.* 1993). Its total luminosity is $V = 16.86 \pm 0.18$. Its half-light radius is $r_h \sim 0\farcs052 \pm 0\farcs010 = 2$ pc.

The virial mass given by r_h and $\sigma = 600$ km s^{-1} is 10^9 M$_\odot$, consistent with the model results. With § 5, this shows that the MDO half-mass radius is $\lesssim r_h$. At $r \leq r_h$, its mean density is 2.5×10^7 M$_\odot$ pc^{-3}. Could the MDO be a cluster of neutron stars or stellar BHs? It has > 50 times the mass of the visible nucleus. To make an MDO cluster, 2×10^9 M$_\odot$ of material must have been delivered to the central 5 pc, turned into massive stars, and thence into remnants. Little of the mass ends up in remnants; the rest is lost. But all of the lost gas must be reused to make more remnants, because if $\gtrsim 50$ % of the mass is thrown away, the cluster becomes unbound. This implies that recycled gas made new stars inside a nucleus with $L \sim 10^{11}$ to 10^{12} L$_\odot$. Conditions did not favor star formation. All this must have happened without over-enriching the visible stars, and it happened quickly enough so those stars can look old. This seems difficult. The requirements are much more stringent than those of the starburst model of quasars (e. g., Terlevich & Boyle 1993), because the active volume is tiny (5 pc versus $\gtrsim$ 100 pc radius). The above is not a rigorous proof that BH alternatives are impossible. But the difficulty of engineering a dark cluster supports our conclusion that NGC 3115 contains a 2×10^9-M$_\odot$ BH.

We are most grateful to C. D. Keyes, J. Christensen, and J. Hayes for help with the data analysis. This work was supported by HST data analysis funds through grant GO–02600.01–87A and by NSERC. Kormendy's ground-based work was supported by NSF grant AST 9219221. Bender's work was supported by SFB 375 of the German Science Foundation and by the Max Planck Gesellschaft.

REFERENCES

Bender, R. 1990, A&A, 229, 441
Bender, R., Saglia, R. P., & Gerhard, O. E. 1994, MNRAS, 269, 785
Dressler, A., & Richstone, D. O. 1988, ApJ, 324, 701
Keyes, C. D., *et al.* 1995, FOS Instrument Handbook (Baltimore: STScI)
Kormendy, J. 1988, ApJ, 325, 128
Kormendy, J., & Richstone, D. 1992, ApJ, 393, 559 (KR92)
Kormendy, J., & Richstone, D. 1995, ARA&A, 33, 581
Kormendy, J., Richstone, D., Gebhardt, K., *et al.* 1996, in preparation
Lauer, T. R., *et al.* 1993, AJ, 106, 1436
Lauer, T. R., *et al.* 1995, AJ, 110, 2622
Richstone, D. O., & Tremaine, S. 1988, ApJ, 327, 82
Scorza, C., & Bender, R. 1995, A&A, 293, 20
Terlevich, R. J., & Boyle, B. J. 1993, MNRAS, 262, 491
van der Marel, R. P., *et al.* 1994, MNRAS, 268, 521

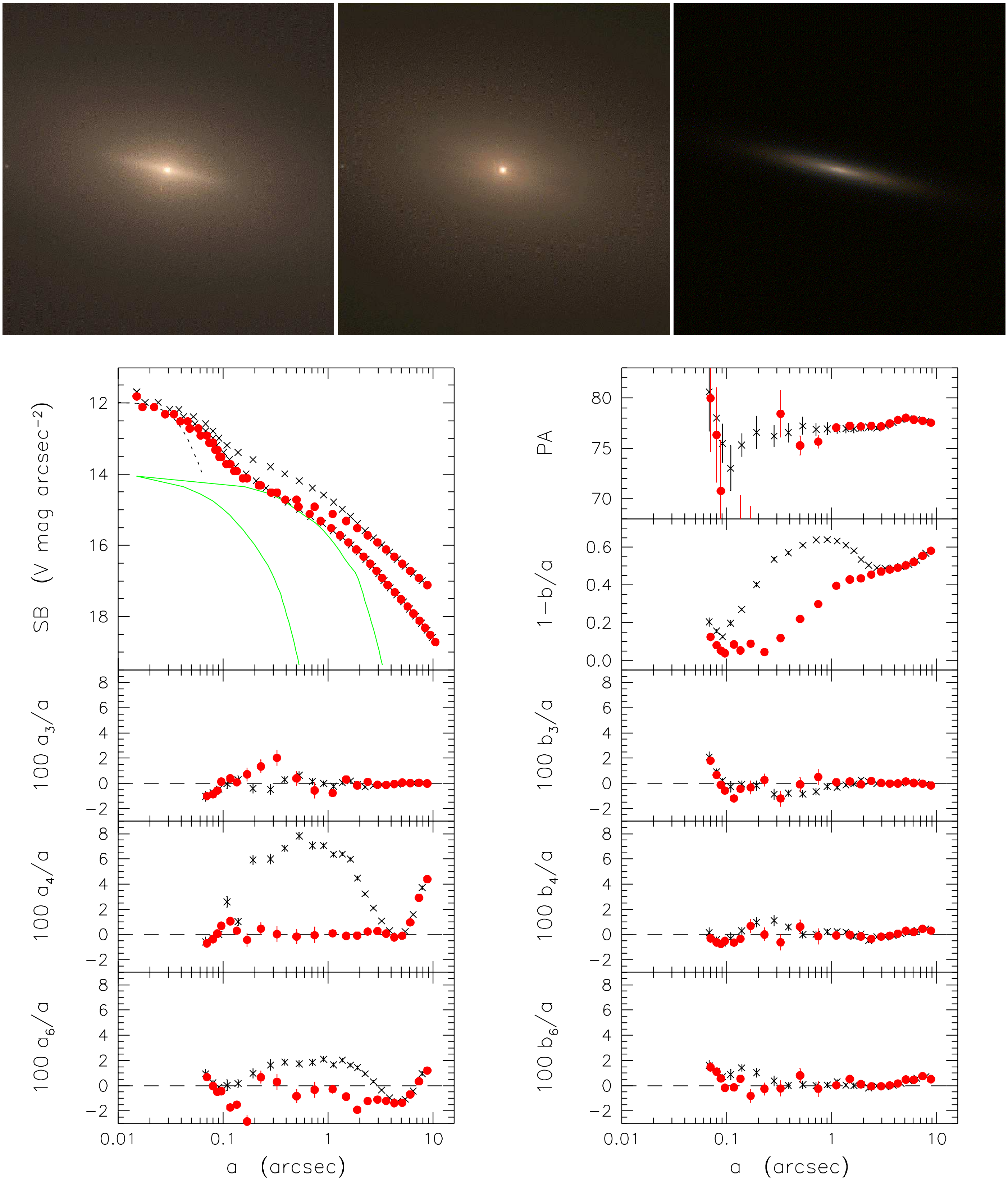

FIG. 4.—(*top*) *HST* WFPC2 images of NGC 3115 obtained 1994, November 3: (*left*) Color image made from 1050 s V- and I-band images; these and the residual PSF (*dotted line in top-left plot*) are after 20 iterations of Lucy deconvolution. (*right*) Inclined disk model that, when subtracted from the raw image, produces a residual image (*center*) with isophotes that are as close to elliptical as possible. Brightness is proportional to the square root of intensity; colors are exaggerated slightly to illustrate the lack of dust and large population gradients. All panels are 11.″6 square. (*bottom*) Bulge isophote parameters as a function of major-axis radius a before (*crosses*) and after (*red filled circles*) disk decomposition. The decomposition technique (Scorza & Bender 1995) finds the best-fitting inclined, thin, and PSF-convolved disk that accounts for the disky isophote distortion. This is measured by a_4/a, i. e. the fractional radial departure along the major axis of the isophotes from best-fitting ellipses. The 7 % distortion due to the nuclear disk disappears after decomposition. Other Fourier distortion coefficients, $a_3 - a_6$ and $b_3 - b_6$, also are small. The top plots show major- and minor-axis surface brightness SB, position angle PA, and ellipticity $1 - b/a$. The disk profiles (*green solid lines*) are almost exponential.